Optics & Laser Technology 163 (2023) 109424

Contents lists available at ScienceDirect

Optics and Laser Technology

journal homepage: www.elsevier.com/locate/optlastec

Full length article

Anti-resonant fiber with nested U-shape tubes for low-loss terahertz waveguides

Guangrong Sun [a,b], Qiang Liu [a,b,*], Haiwei Mu [a,b], Yudan Sun [c], Shimiao Wang [a,b], Mingzhu Han [a,b], Jianxin Wang [a,b], Jingwei Lv [a,b], Paul K. Chu [d], Chao Liu [a,b,*]

[a] SANYA Offshore Oil & Gas Research Institute, Northeast Petroleum University, Sanya 572024, PR China
[b] School of Physics and Electronic Engineering, Northeast Petroleum University, Daqing 163318, PR China
[c] College of Mechanical and Electrical Engineering, Daqing Normal University, Daqing 163712, PR China
[d] Department of Physics, Department of Materials Science and Engineering, and Department of Biomedical Engineering, City University of Hong Kong, Tat Chee Avenue, Kowloon, Hong Kong, China

ARTICLE INFO

Keywords:
Anti-resonant fiber
Terahertz
High-resistivity silicon
Low-loss transmission

ABSTRACT

A novel terahertz anti-resonant fiber is designed and described. The high-resistivity silicon in the fiber mitigating the effective material loss and the nested double-layer U-shape tubes work together to reduce the transmission loss. The confinement loss and effective material loss are analyzed and optimized by the finite element method. The optimized fiber shows a total loss of 3.1×10^{-3} dB/m at 1 THz and the low-loss transmission bandwidth is 0.44 THz in the range of 0.5–1.5 THz. The influence of bending on the transmission loss is analyzed and the bending loss is less than 2.1×10^{-2} dB/m at 1 THz for bending radii bigger than 60 cm. The anti-resonant fiber delivers excellent performance and has high commercial potential in terahertz waveguides.

1. Introduction

The terahertz range, also known as the terahertz gap, spans frequencies from 0.1 to 10 THz corresponding to wavelengths between 30 and 3,000 μm. Compared to electromagnetic waves in other spectral bands, terahertz waves have unique properties such as high transmittance, security, and fingerprint capability [1] and are used in many applications including non-destructive imaging [2], medical examination [3], security surveillance [4], terahertz communication [5], sensing [6], drug testing [7], and military applications [8]. Many terahertz applications require transmission in free space, but terahertz waves traversing in free space are affected critically by ambient and atmospheric conditions. Consequently, the transmission loss can be large thus restricting further development [9]. Therefore, researchers have investigated dielectric waveguides that can be used to transmit terahertz waves, for instance, metallic wires [10], dielectric tubes with metal coatings [11], sub-wavelength fibers [12], porous fibers [13], and hollow core fibers [14]. Among them, hollow core fibers have received extensive attention due to low-loss and low-dispersion transmission.

Hollow core fibers mainly include photonic band gap fibers [15] (HC-PBGF) and anti-resonant fibers [16] (HC-ARF). The HC-PBGF utilizes the photonic bandgap effect formed by the periodic cladding to realize light transmission. Although the HC-PBGF can achieve low-loss transmission, its bandwidth is relatively limited. In comparison, the HC-ARF has outstanding transmission characteristics such as small nonlinearity, low transmission loss, negligible dispersion, as well as large bandwidth [17]. The mechanism is based on the anti-resonant effect by inhibiting coupling between the core mode and cladding modes for light transmission in the near-infrared, mid-infrared, and terahertz regimes. In the terahertz range, silica produces large transmission loss and so some polymeric materials such as Topas [18], Zeonex [19], PMMA [20], HDPE [21], Teflon [22], and PP [23] have been proposed. In particular, PMMA, Topas, and Zeonex have the advantages of low effective material loss and low cost [24]. V. Setti et al. have made a terahertz anti-resonant fiber using PMMA [25] and measured the total loss in the experiment, the value is 16 dB/m at 0.828 THz. G. K. M. Hasanuzzaman et al. have proposed and simulated a terahertz anti-resonant fiber consisting of nested circular tubes composed of Topas [26] with transmission loss lower than that of the non-nested circular tubes. The total loss of the fiber is 0.05 dB/m at 1 THz wherein the confinement loss and the effective material loss are 3.4307×10^{-4} dB/m and 0.05 dB/m respectively. Moreover, the low-loss transmission

* Corresponding authors.
E-mail addresses: nepulq@126.com (Q. Liu), msm-liu@126.com (C. Liu).

https://doi.org/10.1016/j.optlastec.2023.109424
Received 5 July 2022; Received in revised form 16 February 2023; Accepted 24 March 2023

bandwidth is 0.4 THz. A. Mollah et al. have reported and numerically analyzed a terahertz anti-resonant fiber with an asymmetric cladding based on Zeonex [27]. The structure consisting of connecting semi-circular tubes and semi-elliptical tubes shows a total loss of 0.034 dB/m at 1 THz, the confinement loss is on the order of 10^{-4} dB/m and the effective material loss is 0.034 dB/m. In addition, the low-loss transmission bandwidth is 0.5 THz. It is noted that the effective material loss of the aforementioned terahertz anti-resonant fiber is not reduced effectively. Hence, fibers with low effective material loss in the terahertz regime is crucial to the performance. J. Dai et al. have verified the use of high-resistivity silicon (HRS) [28] in the experiment and the material absorption coefficient is less than 1.5 m^{-1} in the 0.1–1.5 THz range. The change of refractive index is only 0.0001 in the range of 0.5–4.5 THz with nearly zero dispersion and the low effective material loss bode well for photonic crystal fibers in the terahertz range [29–31].

Herein, high-resistivity silicon (HRS) is used to design the anti-resonant fiber and the nested double-layer U-shape tubular structure achieves low-loss transmission of terahertz waves. In the range of 0.86–1.2 THz, the effective material loss decreases to the order of 10^{-4} dB/m. Meanwhile, the confinement loss is 2.6×10^{-3} dB/m at 1 THz and the low-loss transmission bandwidth is 0.44 THz. In addition, the anti-resonant fiber exhibits good bending resistance as exemplified by bending loss of less than 2.1×10^{-2} dB/m at 1 THz for bending radii greater than 60 cm. To the best of our knowledge, this novel terahertz anti-resonant fiber is the first one showing a total loss of less than 10^{-2} dB/m.

2. Fiber structure

The anti-resonant fiber is described schematically in Fig. 1. The cladding consists of 6 pairs of U-shape lattice tubes and each U-shape tube is formed by splicing a semi-circular lattice tube and two lattice bars. The white area is air. The core diameter is $D_{core} = 3$ mm and the diameters of the outer and inner layers of the nested U-shape tubes are $d_{tube} = 2.5$ mm and $d_{nest} = 0.9$ mm, respectively. The wall thickness of the nested U-shape tubes is $t = 0.035$ mm. The thickness of the jacket tube is $JT = 0.15$ mm and overall fiber radius is $R = 4.15$ mm. The feasible schemes of manufacturing anti-resonant fiber mainly include stacking method, extrusion method, 3D printing fiber and 3D printing preform. Generally, the stacking method is feasible for the compact cladding tubes structure, such as Ref. [25]. The proposed nested U-shape tubes structure cannot be carried out by the stacking method. The extrusion method and 3D printing fiber can be used to fabricate shorter anti-resonant fiber which is less than several tens of centimeters [32–34]. The 3D printing preform is a promising method for anti-resonant fiber and has been attempted to draw hollow core fiber using the polymer composites with lower melting point [35,36]. It is a potential technology for the proposed anti-resonant fiber based on HRS of higher melting point in the future with the progress of the 3D printing preform technology. In this work, the finite element method (FEM) is used to analyze and optimize the anti-resonant fiber. The modeling of terahertz anti-resonant fiber is crucial, particularly the selection of mesh size is important [37,38]. We used extremely fine mesh sizes in the HRS walls and air regions respectively according to [37,38]. The choice of such mesh sizes provides excellent agreement with the experimental results. Since the low refractive index changing rate of the HRS material is in the range of 0.5–4.5 THz, the refractive index is set to have a constant value of 3.417 [29–31].

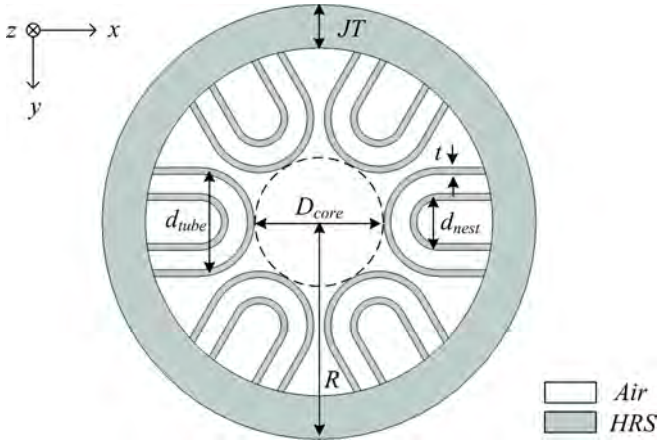

Fig. 1. Cross-section of the anti-resonant fiber.

3. Results and discussion

According to the principle of the HC-ARF, as the core mode matches the cladding modes, there is higher loss of the transmitted light. Therefore, it is necessary to compute and avoid the resonant frequency when designing the anti-resonant fiber, so that light can traverse the anti-resonant region with reduced loss. The resonant frequency can be calculated by Eq. (1) [39]:

$$f_c = \frac{mc}{2t\sqrt{n^2 - 1}} \tag{1}$$

where c is the speed of light in free space, m is the resonant order (positive integer value), n is the refractive index of the HRS material, and t is the wall thickness of the nested U-shape tubes. For $n = 3.417$, $m = 1$, and $t = 0.035$ mm, 0.04 mm, 0.045 mm, and 0.05 mm, the corresponding resonant frequencies f_c are 1.31 THz, 1.14 THz, 1.01 THz, and 0.91 THz, respectively. Hence, the proper wall thickness t is necessary to keep the resonant frequencies away from 1 THz [27].

3.1. Optimization of the wall thickness (t)

Reducing the transmission loss of the fiber is the key to the HC-ARF. The transmission loss of the anti-resonant fiber includes mainly the confinement loss and effective material loss. The confinement loss, also known as leakage loss, refers to the power loss caused by optical field leakage determined by the fiber structure. The loss is intrinsic to the fiber and unavoidable in theory. The confinement loss can be calculated by Eq. (2) [39]:

$$CL = 8.686\left(\frac{2\pi f}{c}\right) Im\left(n_{eff}\right), [dB/m] \tag{2}$$

where c is the speed of light in free space, f is the operating frequency, and $Im(n_{eff})$ is the imaginary part of the effective refractive index. Note that the absorption loss of air is ultra-low and can be neglected in the following simulations. Thus, we only take the absorption caused by HRS into account [40]. The effective material loss of HRS can be expressed by Eq. (3) [24,27]:

$$EML = 4.34\sqrt{\frac{\varepsilon_0}{\mu_0}}\frac{\int_{A_{mat}} n\alpha_{mat}|E|^2 dA}{2\int_{All} S_z dA}, [dB/m] \tag{3}$$

where ε_0 and μ_0 are the permittivity and permeability in free space, respectively and n and α_{mat} are the refractive index and material absorption coefficient of HRS, respectively. S_z is the z-component of the Poynting vector and can be expressed as $S_z = \frac{1}{2}Re(E \times H^*)z$, where E is the electric field and H is the magnetic field.

Initially, the effect of the wall thickness t of the nested U-shape tubes on the loss spectra of the anti-resonant fiber is investigated. For $R = 4.15$ mm, $JT = 0.15$ mm, $D_{core} = 3$ mm, $d_{tube} = 2.5$ mm, and $d_{nest} = 0.9$ mm, the confinement loss spectra for different wall thicknesses are exhibited in Fig. 2(a). As the wall thickness t decreases, the low-loss region (less than10^{-1} dB/m) shifts gradually towards high frequencies. The loss

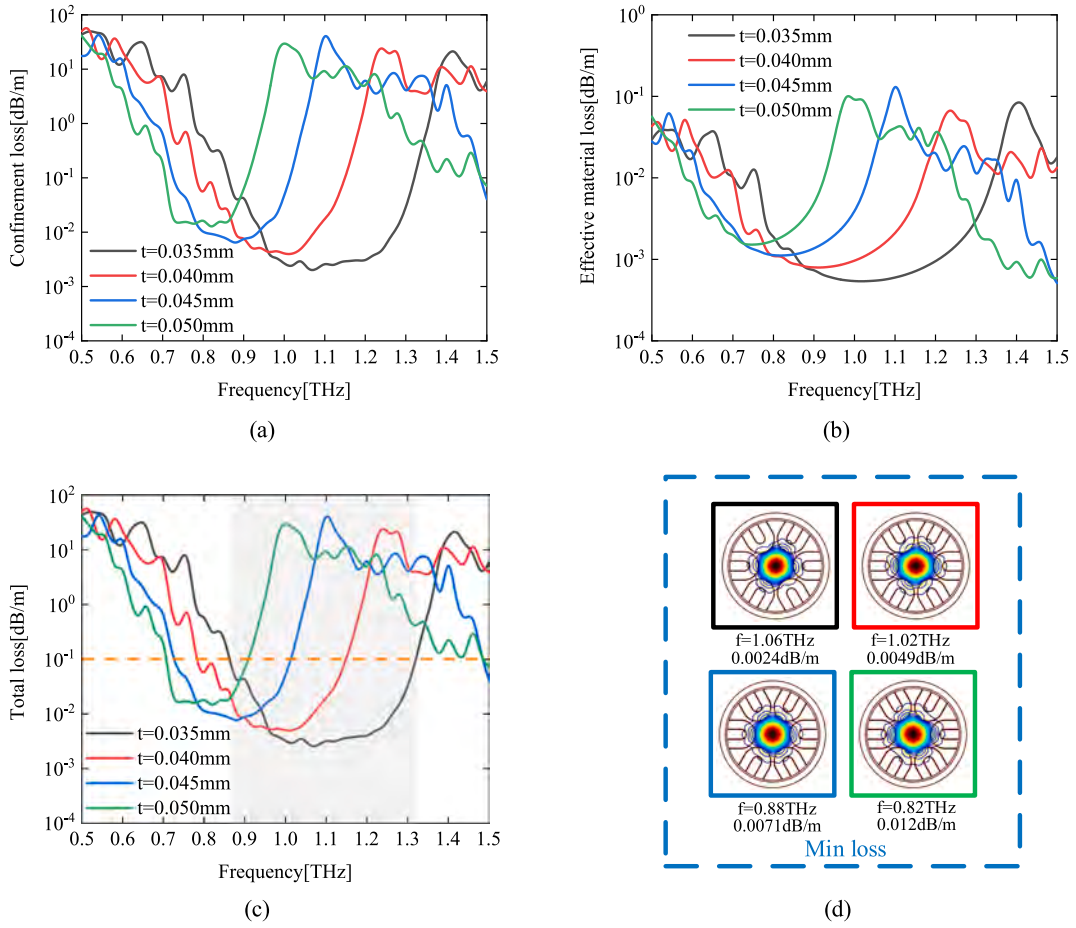

Fig. 2. Transmission characteristics of the structure with different wall thickness *t*: (a) Confinement loss, (b) Effective material loss, (c) Total loss and (d) Contour plots of the electric field for minimum loss.

decreases gradually and bandwidth widens. This is because a smaller wall thickness results in a higher resonant frequency and wider low-loss region [27]. When $t = 0.035$ mm, the low-loss region in the confinement loss spectra is the widest and the minimum confinement loss is 1.9×10^{-3} dB/m.

The effective material loss spectra for different wall thicknesses are presented in Fig. 2(b). With decreasing the wall thickness *t*, the low-loss region moves gradually to the high frequency direction and the minimum effective material loss is 5×10^{-4} dB/m, which is significantly better those observed from other polymeric materials [25–27]. It is because that the effective material loss is determined by the material absorption coefficient according to Eq. (3). The material absorption coefficient of HRS is only less than 1.5 m^{-1} in the 0.1–1.5 THz range which is much less than that of 27.6 m^{-1} and 20 m^{-1} for Topas [26] and Zeonex [27] around 1 THz. Therefore, HRS reduces the effective material loss of the anti-resonant fiber leading to low-loss transmission.

The total loss is the superposition of the confinement loss and effective material loss and in this case, mainly depends on the confinement loss. The total loss spectra for different wall thicknesses are depicted in Fig. 2(c). As $t = 0.035$ mm, the anti-resonant fiber shows the lowest total loss of 2.4×10^{-3} dB/m and the largest low-loss transmission bandwidth ($<10^{-1}$ dB/m) of 0.44 THz. Fig. 2(d) presents the contour plots of the electric field of the lowest loss for different wall thicknesses. The light field is confined in the core region and as the wall thickness *t* decreases, the minimum loss decreases.

3.2. Optimization of the outer and inner layer diameters (d_{tube} and d_{nest})

Next, for $R = 4.15$ mm, $JT = 0.15$ mm, $D_{core} = 3$ mm, $d_{nest} = 0.9$ mm, and $t = 0.035$ mm, the total loss spectra for different outer layer diameters are shown in Fig. 3(a). As d_{tube} changes from 1.9 mm to 2.5 mm, the minimum loss and low-loss bandwidth change only slightly, implying that the outer layer diameter has little effect on the total loss.

Fig. 3(b) shows the confinement loss, effective material loss, and total loss for different outer layer diameters at 1 THz. The confinement loss changes slowly with increasing outer layer diameter d_{tube} and the drop fluctuates. In the range of 1.7–2.7 mm, the changing rate of the effective material loss is only -2.1×10^{-5}, showing that the outer layer diameter hardly affects the effective material loss. The solid blue line is the total loss and the insets show the contour plots of the electric field for different outer layer diameters. It can be seen that the light field is well confined in the core region and the total loss does not change much. In practice, a bigger outer layer diameter affects the flexibility of the fiber consequently impacting the bending resistance [26]. Therefore, the bending loss of *x* direction is calculated at 1 THz as the bending radii R_b is 40 cm. Considering the smaller bending loss and lowest total loss at 1 THz, $d_{tube} = 2.5$ mm is chosen as the optimal value.

We also examine the effect of the inner layer diameter d_{nest} of the nested U-shape tubes on the loss spectra. For $d_{tube} = 2.5$ mm, the total loss spectra for different inner layer diameters are shown in Fig. 4(a). The inner layer diameter significantly affects the minimum loss and low-loss bandwidth. When the inner U-shape tube is removed ($d_{nest} = 0$ mm), the anti-resonant fiber exhibits a bigger total loss with the smallest value being 2.3×10^{-1} dB/m. At the same time, the inset of Fig. 4(b) marked by the red frame shows the contour plots of the electric field. It is evident that light leak into the cladding region and the total loss is relatively large.

After adding the inner layer nested U-shape tubes, the light field is

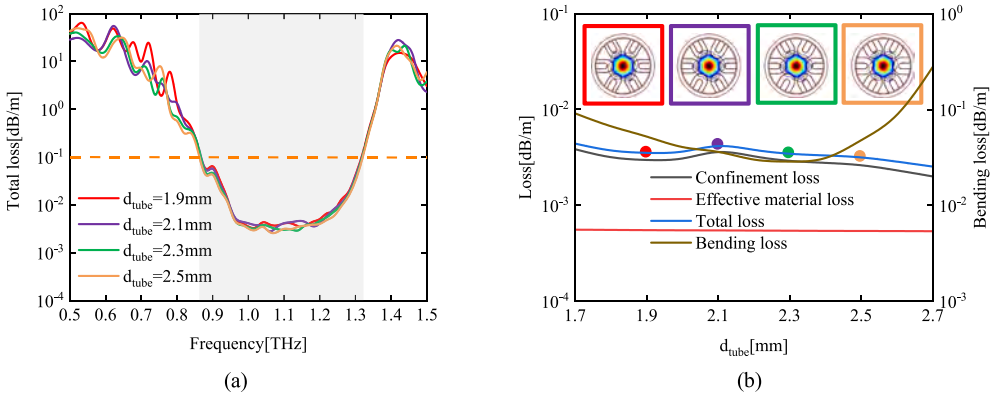

Fig. 3. Effect of the outer layer diameter d_{tube} on loss: (a) Total loss versus frequencies and (b) Loss and bending loss for different outer layer diameters for $f = 1$ THz.

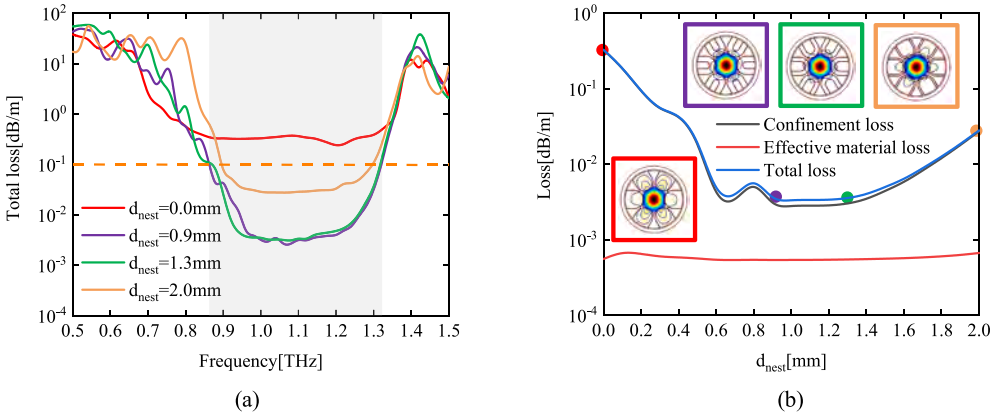

Fig. 4. Effect of the inner layer diameter d_{nest} on loss: (a) Total loss versus frequencies and (b) Loss for different inner layer diameters at $f = 1$ THz.

well confined in the core region and the total loss decreases significantly, as shown in the other insets in Fig. 4(b). This is because that the inner layer nested U-shape tubes provide a second anti-resonant layer to enhance the anti-resonant effect [41]. As $d_{nest} = 0.9$ mm and 1.3 mm, the total loss is similar, especially in the low-loss region as shown in Fig. 4 (a). Meanwhile, Fig. 4(b) shows the confinement loss, effective material loss, and total loss for different inner layer diameters at 1 THz and the inner layer diameter has little effect on the effective material loss but mainly affects the confinement loss. In the range of 0–2 mm, the total loss decreases rapidly and then increases slowly. Based on the lowest total loss at 1 THz, $d_{nest} = 0.9$ mm is chosen as the optimal value.

3.3. Loss comparison for different numbers of tubes

Furthermore, we discuss the effect of the number of the nested U-shape tubes on the loss spectra as illustrated in Fig. 5. For $R = 4.15$ mm, $JT = 0.15$ mm, $D_{core} = 3$ mm, $d_{tube} = 2.5$ mm, $d_{nest} = 0.9$ mm, and $t = 0.035$ mm, the total loss spectrum for the four-tube structure shows a bigger loss, which can be explained by the contour plots of the electric field (black block) at 1 THz. It is evident that the light field is not confined in the core region. When the number of the nested U-shape tubes increases to five, the light field is confined in the core region. The six nested U-shaped tubes further enhance the anti-resonant effect and thus show a smaller total loss. It is because the more the number of tubes, the closer the adjacent tubes are and the harder for light to leak through the gaps [42]. Therefore, the light field is confined to the core region thus enabling low-loss transmission.

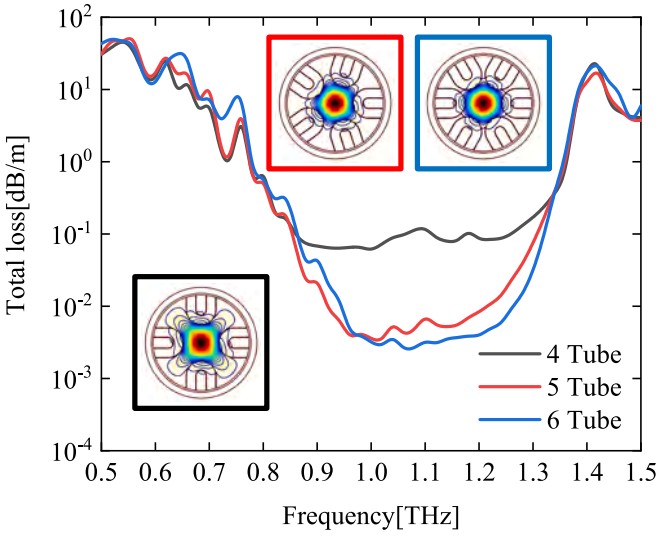

Fig. 5. Total loss for different numbers of tubes.

3.4. Bending effect

In practice, bending is common and inevitably increases the loss. Hence, controlling the bending loss of anti-resonant fibers is important. To calculate the bending loss, we use a conformal transformation method to modify the refractive index of an equivalent straight fiber as shown by Eq. (4) [43,44]:

$$n_{eq} = ne^{\frac{u}{R_b}} \quad (4)$$

where R_b is the bending radius, u is the bending direction of the fiber (x or y), n is the refractive index of the straight fiber, and n_{eq} is the equivalent refractive index of the fiber after bending. The bending loss can be calculated by taking the n_{eq} into Eq. (2).

Finally, the bending loss of the proposed anti-resonant fiber is studied. Fig. 6(a) shows the bending loss spectra of x direction for different bending radii. The minimum loss increases with decreasing bending radius R_b and the low-loss bandwidth also decreases. For the bending radius R_b = 30 cm, there is almost no low-loss region in the entire terahertz range and almost all the bending loss is larger than 10^{-1} dB/m. This is because the symmetrical structure of the anti-resonant fiber is destroyed by bending. Consequently, the refractive index profile is distorted and the confinement loss enhances compared to a straight fiber [9]. To further study the bending performance of the anti-resonant fiber, we analyze the bending loss of x direction for different bending radii at 1 THz as shown in Fig. 6(b). When the bending radius is relatively large, the light field is confined in the core as shown in the insets (green and purple blocks). Although bending causes the light field to be off-center, it does not result in obvious leakage and so the bending loss is relatively small. The anti-resonant fiber shows good bending resistance. As the bending radius R_b decreases, the bending loss increases gradually and appears extra loss peak with 1.6×10^{1} dB/m as R_b = 30 cm. The extra loss is due to the resonances between the core mode and cladding modes when the modes are phase matched [25] as shown in the blue inset.

Similarly, the bending loss spectra of y direction are shown in Fig. 6(c). Compared with the loss spectra of x direction, the low-loss bandwidth and the minimum loss exhibit same change trend with changing bending radiusR_b. The bending loss of y direction is a little bigger than that of x direction at 1 THz as shown in Fig. 6(d), but still maintained at a lower level. Compared to Ref [9], this anti-resonant fiber has better and more robust transmission characteristics.

4. Conclusion

An anti-resonant fiber composed of nested double-layer U-shape tubes constructed with high-resistivity silicon is designed and analyzed. The high-resistivity silicon mitigates the effective material loss in the terahertz regime. By optimizing the structure, the anti-resonant fiber exhibits extremely low total loss and relatively large low-loss bandwidth in the range of 0.5–1.5 THz. The total loss is 3.1×10^{-3} dB/m at 1 THz and the low-loss transmission bandwidth is 0.44 THz. Furthermore, the fiber shows excellent bending resistance with bending loss of less than 2.1×10^{-2} dB/m at 1 THz for bending radii greater than 60 cm. The excellent properties suggest that the anti-resonant fiber has large potential in terahertz waveguides.

CRediT authorship contribution statement

Guangrong Sun: Ideas, Conceptualization, Methodology, Software, Investigation, Formal Analysis, Writing. **Qiang Liu:** Ideas, Conceptualization, Methodology, Software, Investigation, Formal Analysis, Writing, Corresponding Author. **Haiwei Mu:** Resources. **Yudan Sun:** Management. **Shimiao Wang:** Software. **Mingzhu Han:** Data Curation. **Jianxin Wang:** Supervision. **Jingwei Lv:** Investigation. **Paul K. Chu:** Article polishing. **Chao Liu:** Resources, Article polishing, Corresponding Author.

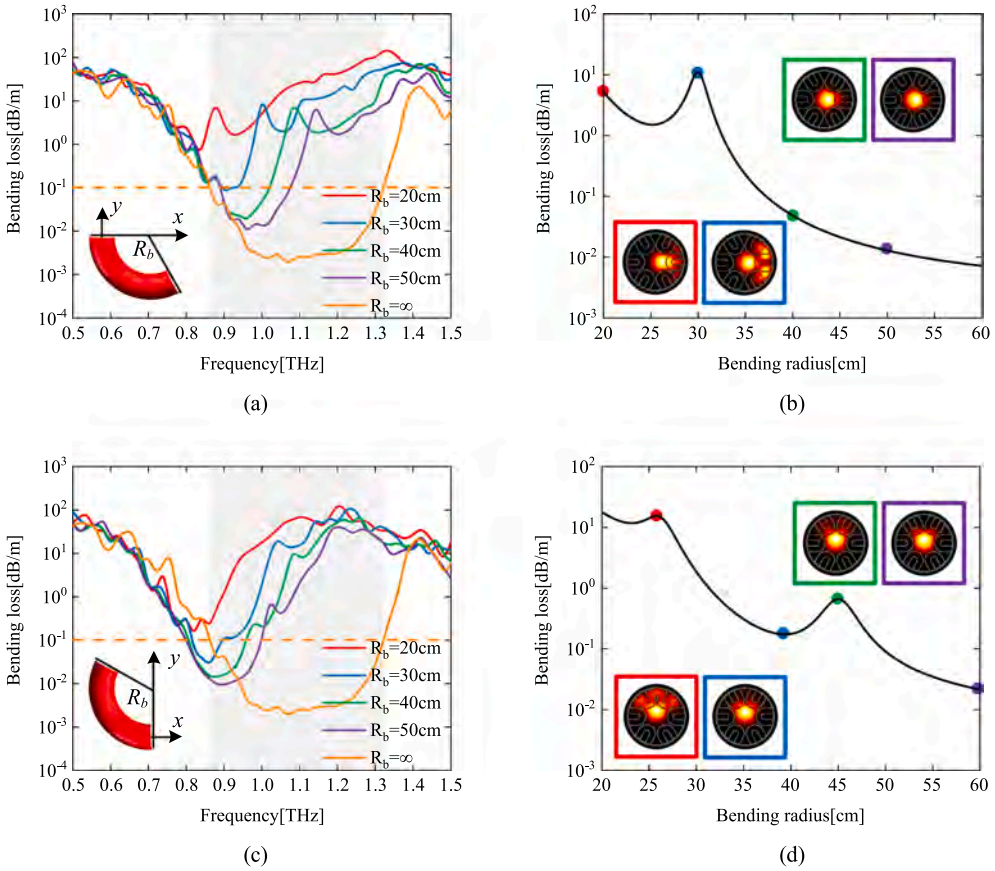

Fig. 6. (a) Bending loss of × direction versus frequencies for different bending radii, (b) Bending loss of × direction versus radii at f = 1 THz, (c) Bending loss of y direction versus frequencies for different bending radii and (d) Bending loss of y direction versus radii at f = 1 THz.

Declaration of Competing Interest

The authors declare that they have no known competing financial interests or personal relationships that could have appeared to influence the work reported in this paper.

Data availability

The data that has been used is confidential.

Acknowledgements

This work was jointly supported by the Provincial Talent Project [ts26180221], Hainan Province Science and Technology Special Fund [ZDYF2022GXJS003], Youth Science Foundation of Northeast Petroleum University [2019QNL-17], Local Universities Reformation and Development Personnel Training Supporting Project from Central Authorities, Natural Science Foundation of Heilongjiang Province [grant number LH2021F007], China Postdoctoral Science Foundation funded project [grant number 2020M670881], City University of Hong Kong Strategic Research Grant (SRG) [grant number 7005505], City University of Hong Kong Donation Research Grant [grant number DON-RMG 9229021].

References

[1] S. Islam, C.M.B. Cordeiro, M.A.R. Franco, Terahertz optical fibers [Invited], Opt. Express 28 (11) (2020) 16089–16117.
[2] K. Kawase, Y. Ogawa, Y. Watanabe, Non-destructive terahertz imaging of illicit drugs using spectral fingerprints, Opt. Express 11 (20) (2003) 2549–2554.
[3] C.J. Strachan, P.F. Taday, D.A. Newnham, Using terahertz pulsed spectroscopy to quantify pharmaceutical polymorphism and crystallinity, J. Pharm. Sci. 94 (4) (2005) 837–846.
[4] N. Laman, S.S. Harsha, D. Grischkowsky, 7 GHz resolution waveguide THz spectroscopy of explosives related solids showing new features, Opt. Express 16 (6) (2008) 4094–4105.
[5] A. Barh, B.P. Pal, G.P. Agrawal, Specialty fibers for terahertz generation and transmission: a review, IEEE J. Sel. Top. Quant. 22 (2) (2016) 8500215.
[6] D. Abbott, X. Zhang, Scanning the Issue: T-Ray imaging, sensing, and retection, P. IEEE 95 (8) (2007) 1509–1513.
[7] M. Nagel, P.H. Bolivar, M. Brucherseifer, Integrated THz technology for label-free genetic diagnostics, Appl. Phys. Lett. 80 (1) (2002) 154–156.
[8] D.J. Cook, B.K. Decker, M.G. Allen, Quantitative THz spectroscopy of explosive materials, Opt. Terahertz Sci. Technol. (2005).
[9] J. Sultana, S. Islam, C.M.B. Cordeiro, Exploring low loss and single mode in antiresonant tube lattice terahertz fibers, IEEE Access. 8 (2020) 113309–113317.
[10] K. Wang, D.M. Mittleman, Metal wires for terahertz wave guiding, Nature 432 (2004) 376–379.
[11] B. Bowden, J.A. Harrington, O. Mitrofanov, Fabrication of terahertz hollow-glass metallic waveguides with inner dielectric coatings, J. Appl. Phys. 104 (9) (2008), 093110.
[12] J.Y. Lu, C.M. Chiu, C.C. Kuo, Terahertz scanning imaging with a subwavelength plastic fiber, Appl. Phys. Lett. 92 (8) (2008), 084102.
[13] A. Hassani, A. Dupuis, M. Skorobogatiy, Low loss porous terahertz fibers containing multiple subwavelength holes, Appl. Phys. Lett. 92 (7) (2008), 071101.
[14] R. Yu, Y. Chen, L. Shui, Hollow-core photonic crystal fiber gas sensing, Sensors 20 (10) (2020) 20102996.
[15] L. Vincetti, Hollow core photonic band gap fiber for THz applications, Microw. Opt. Techn. Let. 51 (7) (2009) 1711–1714.
[16] S. Gao, Y. Wang, W. Ding, Hollow-core conjoined-tube negative-curvature fibre with ultralow loss, Nat. Commun. 9 (2018) 2828.
[17] J. Sultana, S. Islam, C.M.B. Cordeiro, Terahertz hollow core antiresonant fiber with metamaterial cladding, Fibers 8 (20) (2020) 8020014.
[18] M. Meng, D. Yan, Z. Yuan, Novel double negative curvature elliptical aperture core fiber for terahertz wave transmission, J. Phys. D Appl. Phys. 54 (2021), 235102.
[19] A. Mollah, S. Rana, H. Subbaraman, Polarization filter realization using low-loss hollow-core anti-resonant fiber in THz regime, Results Phys. 17 (2020), 103092.
[20] D. Yan, J. Li, Design and analysis of the influence of cladding tubes on novel THz waveguide, Optik 180 (2019) 824–831.
[21] D. Yan, J. Li, Effect of tube wall thickness on the confinement loss, power fraction and bandwidth of terahertz negative curvature fibers, Optik 178 (2019) 717–722.
[22] V. Kumar, R.K. Varshney, S. Kumar, Terahertz generation by four-wave mixing and guidance in diatomic teflon photonic crystal fibers, Opt. Commun. 454 (2020), 124460.
[23] S. Ariyoshi, S. Hashimoto, S. Ohnishi, Broadband terahertz spectroscopy of cellulose nanofiber-reinforced polypropylenes, Mater. Sci. Eng. B 265 (2021), 115000.
[24] I.M. Ankan, A. Mollah, J. Sultana, Negative curvature hollow-core anti-resonant fiber for terahertz sensing, Appl. Opt. 59 (28) (2020) 8519–8525.
[25] V. Setti, L. Vincetti, A. Argyros, Flexible tube lattice fibers for terahertz applications, Opt. Express 21 (3) (2013) 3388–3399.
[26] G.K.M. Hasanuzzaman, S. Iezekie, C. Markos, Hollow-core fiber with nested anti-resonant tubes for low-loss THz guidance, Opt. Commun. 426 (2018) 477–482.
[27] A. Mollah, S. Habib, S. Habib, Novel hollow-core asymmetric conjoined-tube anti-resonant fiber for low-loss THz wave guidance, OSA Continuum 3 (5) (2020) 1169–1176.
[28] J. Dai, J. Zhang, W. Zhang, Terahertz time-domain spectroscopy characterization of the far-infrared absorption and index of refraction of high-resistivity, float-zone silicon, J. Opt. Soc. Am. B 21 (7) (2004) 1379–1386.
[29] B. Wang, F. Tian, G. Liu, A modified single-polarization THz fiber with epsilon-near-zero (ENZ) material, Res. Optics 1 (2020), 100034.
[30] T. Yang, C. Ding, R.W. Ziolkowski, Circular hole ENZ photonic crystal fibers exhibit high birefringence, Opt. Express 26 (13) (2018) 17264–17278.
[31] T. Yang, C. Ding, R.W. Ziolkowski, A scalable THz photonic crystal fiber with partially-slotted core that exhibits improved birefringence and reduced Loss, J. Lightwave Technol. 36 (16) (2018) 3408–3417.
[32] W. Talataisong, J. Gorecki, L.D.V. Putten, Hollow-core antiresonant terahertz fiber-based TOPAS extruded from a 3D printer using a metal 3D printed nozzle, Photonics Res. 9 (8) (2021) 1513–1521.
[33] S. Yang, X. Sheng, G. Zhao, 3D printed effective single-mode terahertz antiresonant hollow core fiber, IEEE Access. 9 (2021) 29599–29608.
[34] A.L.S. Cruz, C.M.B. Cordeiro, M.A.R. Franco, 3D printed hollow-core terahertz fibers, Fibers 6 (30) (2018) 6030043.
[35] W. Talataisong, R. Ismaeel, T.H.R. Marques, Mid-IR hollow-core microstructured fiber drawn from a 3D printed PETG preform, Sci. Rep. 8 (2018) 8113.
[36] M.G. Zubel, A. Fasano, G. Woyessa, 3D-printed PMMA preform for hollow-core POF drawing, in: The 25th International Conference on Plastic Optical Fibers, 2016, pp. 295–300.
[37] S. Habib, A.I. Adamu, C. Markos, Enhanced birefringence in conventional and hybrid anti-resonant hollow-core fibers, Opt. Express 29 (8) (2021) 12516–12530.
[38] S. Habib, J.E.A. Lopez, C. Markos, Single-mode, low loss hollow-core anti-resonant fiber designs, Opt. Express 27 (4) (2019) 3824–3836.
[39] S. Hossain, A. Mollah, K. Hosain, THz spectroscopic sensing of liquid chemicals using hollow-core anti-resonant fiber, OSA Continuum 4 (2) (2021) 621–632.
[40] Z. Du, Y. Zhou, S. Luo, Highly birefringent hollow-core anti-resonant terahertz fiber with a thin strut microstructure, Opt. Express 30 (31) (2022) 3783.
[41] C. Wei, J. Hu, C.R. Menyuk, Comparison of loss in silica and chalcogenide negative curvature fibers as the wavelength varies, Front. Phys. 4 (30) (2016) 00030.
[42] C. Wei, C.R. Menyuk, J. Hu, Geometry of chalcogenide negative curvature fibers for CO_2 laser transmission, Fibers 6 (40) (2018) 6040074.
[43] S. Habib, O. Bang, M. Bache, Low-loss hollow-core silica fibers with adjacent nested anti-resonant tubes, Opt. Express 23 (13) (2015) 17394–17406.
[44] F. Poletti, Nested antiresonant nodeless hollow core fiber, Opt. Express 22 (20) (2014) 23807–23828.